資　料

Time-course temperature change of refrigerated phantoms during magnetic resonance imaging (MRI): Simulation for postmortem MRI setting

冷蔵ファントムのMRI撮像中の経時的温度変化：死後MRI撮像のシミュレーション

KOBAYASHI Tomoya[1, 2, 3)]*, SHIOTANI Seiji[4)], MURANAKA Hiroyuki[5)], NUMANO Tomokazu[2)], UEDA Takuya[6)], HAYAKAWA Hideyuki[7)], OKUDA Takahisa[3)]

1）Department of Diagnostic Imaging, Graduate School of Medicine, Tohoku University
2）Department of Radiological Sciences, Graduate School of Human Health Sciences, Tokyo Metropolitan University
3）Department of Legal Medicine, Nihon University School of Medicine
4）Department of Radiology, Seirei Fuji Hospital
5）Department of Health Sciences, School of Health Sciences, Nippon Bunri University
6）Department of Diagnostic Radiology, Graduate School of Medicine, Tohoku University
7）Department of Forensic Medicine, Tsukuba Medical Examiner's Office

Key words: postmortem magnetic resonance imaging (MRI), phantom study, refrigerated corpse, radiofrequency heating, temperature

【Abstract】
Radiofrequency (RF) energy-induced heating effect of postmortem MRI is expected to be greater than that of clinical MRI, since physiological temperature control functions are absent in deceased bodies and total examination time tends to be longer. We used head and trunk phantoms kept in cold storage at 4℃ and a 1.5T MR scanner to simulate a refrigerated corpse being examined in a scan room where the ambient temperature is maintained at 23℃. Near surface temperature was measured at 4 points on the phantoms (the head and upper, middle, and lower parts of the trunk) every 5 minutes for 1 hour during scanning and 1 hour after scanning. Whole body average specific absorption rate (SAR) for 6 minutes was calculated in each applied sequence. At the baseline, the head phantom's temperature was lower than the trunk phantom. Though temperatures in all measured points were almost proportional to the time during measurement, the inclination on the temperature/time graph of the head phantom was greater than that of the trunk phantom. The coefficient of determination of the head phantom was 0.998. Meanwhile, the measured temperatures of the trunk phantom were higher than the linear function approximated using least squares method from 30 to 85 minutes after starting MRI. Mean whole body average SAR for 6 minutes was 1.34 ± 1.33 W/kg. RF energy-induced heating effect is expected to occur especially in the trunk of a refrigerated body due to high SAR and a long scanning time.

【要 旨】
死後MRI検査では，生体の体温調節機能が欠如しているため，ラジオ波（RF）エネルギーによる加熱効果が大きく，長時間の撮像により発熱リスクが高まる．われわれは，4℃に冷蔵した頭部および胴体ファントムを使用し，23℃に保たれたMRI検査室で1.5T MRI撮像シミュレーションを行い，表面温度の変化と全身平均比吸収率（SAR）を測定した．その結果，胴体の温度上昇は頭部に比して緩徐であったものの，撮像開始後約30分以降から撮像終了までの間，胴体の温度は予測値をわずかに超過した．平均比吸収率（SAR）は1.34 ± 1.33 W/kgであり，胴体ではRFエネルギーによる熱蓄積が観察され，加熱効果の存在が示唆された．

小林 智哉[1, 2, 3)]*，塩谷 清司（医師）[4)]，村中 博幸[5)]，沼野 智一[2)]，植田 琢也（医師）[6)]，早川 秀幸（医師）[7)]，奥田 貴久（医師）[3)]

1）東北大学大学院　医学系研究科　画像診断学分野
2）東京都立大学　保健福祉学部　放射線学科
3）日本大学　医学部　社会医学系　法医学分野
4）聖隷富士病院　放射線科
5）日本文理大学　保健医療学部
6）東北大学大学院　医学系研究科　放射線診断学分野
7）筑波剖検センター
＊ E-mail: t.kobayashi1001@gmail.com

Received October 28, 2024; accepted April 19, 2025

Introduction

Postmortem magnetic resonance imaging (PMMRI) has increasingly been utilized as a complementary diagnostic tool to postmortem computed tomography (PMCT) [1)], especially in cases where PMCT alone cannot adequately identify or diagnose specific conditions such as myocardial infarction, spinal cord injuries, and congenital abnormalities in pediatric cases [2-4)].

In magnetic resonance imaging (MRI) examinations, most of the radiofrequency

(RF) energy is converted into heat within the patient and it is measured as the specific absorption rate (SAR), the power absorbed per mass of tissue (W/kg) [5]. Rapidly alternating magnetic fields during RF exposure induce eddy currents within the patient's tissue according to Faraday's law of electromagnetic induction. This eddy current generates Joule heat which is proportional to the square of the current and the resistance. Due to the skin effect, eddy current density is highest near the surface, decreasing exponentially with greater depth [6,7]. Consequently, RF energy-induced heating is more pronounced near the body surface, causing greater temperature elevations in superficial areas [8,9]. Indeed, previous reports have shown that RF exposure can increase surface temperatures of the living human body by an average of approximately 0.6℃, with increases of up to 2.1℃ in some cases [10].

RF energy-induced heating effect of PMMRI is expected to become stronger than that in clinical MRI, since physiological temperature control functions are absent in deceased bodies and the total time of whole-body PMMRI tends to be longer than that of MRI of a living patient in clinical settings. In fact, Kobayashi et al. reported that certain regions exhibited skin temperature increase of approximately 8℃ after whole body PMMRI of a refrigerated corpse [11]. This observation raises the possibility that even higher temperature elevations could occur during imaging, posing a risk of surface tissue damage.

A significant concern in PMMRI is thus the heating effect caused by RF exposure during the imaging process, as elevated tissue temperatures can potentially lead to surface tissue damage. To address these issues, it is necessary to capture and analyze temporal temperature changes occurring throughout the PMMRI procedure. Although prior studies have investigated temperature variations only before and after PMMRI of refrigerated cadavers [11], continuous temperature monitoring throughout the imaging process itself has not yet been reported.

The aim of this phantom study, therefore, was to simulate and evaluate the temporal temperature changes occurring during PMMRI of refrigerated cadavers, with a particular focus on assessing the potential risk of surface tissue damage. By providing a detailed analysis of these temperature variations, we aim to offer fundamental insights that will support safer implementation of PMMRI procedures.

Materials and Methods

Subjects

Referencing a trunk phantom of an American Society for Testing and Materials (ASTM) , our experiments were performed using a self-made rectangular prism-shaped trunk phantom with dimensions of 308 mm (width: W) × 540 mm (length: L) × 200 mm (depth: D) surrounded by 12.5-mm-thick acrylic walls, and an oval-shaped head phantom including a nose in the center and a neck portion with dimensions of 178 mm (W) × 279 mm (L) × 265 mm (D) surrounded by a 3-mm-thick polypropylene wall (Fig. 1). The trunk phantom (26.6 kg)

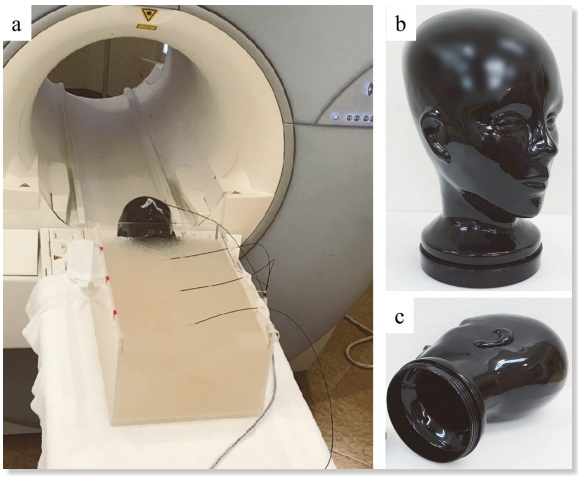

Fig. 1 Head and trunk phantoms and 4 fiber-optic thermometers

(a) Head and trunk phantoms placed in the MRI scanner, with 4 fiber-optic thermometers inserted into the trunk phantom for temperature measurement. (b,c) Close-up view of the black head phantom used in the study.

and the head phantom (5.6 kg) were securely adhered using a waterproof adhesive to ensure close contact. The phantoms were then filled with a sol which was prepared using 26.6 ℓ deionized water, 35.1 g of NaCl, and 266.1 g of polyacrylic acid (PAA). The prepared sol, which had a conductivity (σ) of 0.49 S/m and dielectric constant (ε) of 78 according to the procedures described in the ASTM standard [12], was infused into the head and trunk phantoms to a depth of 180 mm. Though we did not perform a degassing operation to eliminate air bubbles in the prepared sol, we visually confirmed the absence of air bubbles. In this study, we considered non-decomposed cadavers to have material properties nearly equivalent to those of living bodies, as advanced decomposition is not typically observed in routine PMMRI. After having been kept in cold storage at 4℃ for 11 hours, a standard temperature widely used to maintain tissue flexibility and slow down tissue degradation in cadavers [13], MRI was performed on the head and trunk phantoms.

Measurement of temperature

We measured temperature of the phantoms using 4 fiber optic thermometers (FL2400-4ch, Anritsu Meter Co. Ltd., Tokyo, Japan) with an accuracy and resolution of 0.1℃. These thermometers were composed of optical fibers 10 meters in length and were not influenced by magnetic field or RF irradiation. The absolute values of the fiber optic temperature sensors were calibrated with a thermocouple thermometer. Temperatures at 4 points on the phantoms at a depth of 10 mm from the surface were measured to avoid the effects of evaporative heat loss (Figs. 1-3). This depth was chosen as it is sufficiently close to the surface to accurately reflect temperature changes influenced by RF energy, which are known to be greatest near the surface due to the skin effect, while simultaneously ensuring stable and consistent measurements. Exact

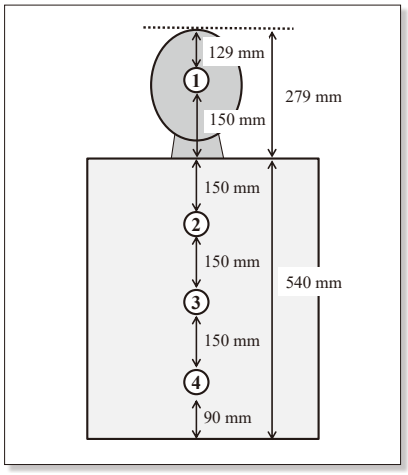

Fig. 2 Temperature measurement points on the phantoms

Four points set on the phantoms for near surface temperature measurement
① Head phantom
② Upper part of the trunk phantom
③ Middle part of the trunk phantom
④ Lower part of the trunk phantom

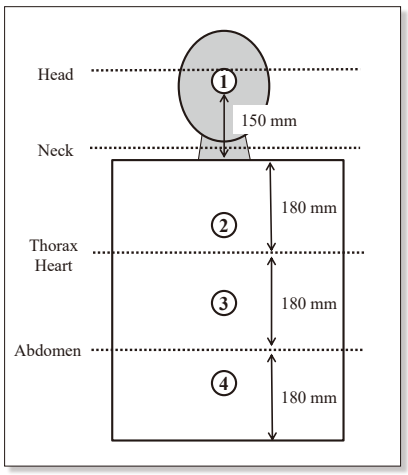

Fig. 3 Temperature measurement points and centers of the static magnetic field (B_0) for 4 scanned sites

Center of the static magnetic field for each part of the phantom
Head: One-third from the top of the head phantom excluding the neck
Neck: Middle of the neck
Thorax, Heart: One-third from the top of the trunk phantom
Abdomen: Two-thirds from the top of the trunk phantom
(①②③④ indicate the point of temperature measurement)

locations of the 4 measured points were set as follows:

① Head phantom: At the central nose (a fiber optic thermometer was inserted into the

prepared sol through a 10 mm-diameter hole created on the top of the surface).

② Upper part of the trunk phantom: At the point where the anterior midline of the phantom and the line at 150 mm caudal direction from the top of the phantom intersect.

③ Middle part of the trunk phantom: At the point where the anterior midline of the phantom and the line at 300 mm caudal direction from the top of the phantom intersect.

④ Lower part of the trunk phantom: At the point where the anterior midline of the phantom and the line at 450 mm caudal direction from the top of the phantom intersect.

In our study, the temperature measurement was conducted on the head and trunk phantoms without extremities (arms and legs) for the following reasons:

- The ASTM head and trunk phantom we referenced was designed without assuming its application for the extremities.
- Only four fiber optic temperature sensors were available for the experiment.
- Generally, lethal lesions exist in the head or trunk of a deceased body.

The temperature was measured every 5 minutes from immediately before starting the scan till 60 minutes after completion of scan to evaluate both the influence of the RF energy-induced heating effect and the ambient temperature.

Ambient conditions

The ambient temperatures of the magnetic bore and the scan room were maintained at 23.0℃ during the entire procedure. To measure near surface temperature distribution caused by RF energy-induced heating effect, the cooling fan of the MR unit was switched off.

MRI examination

MRI was performed using a 1.5T unit (Avanto, Siemens, Erlangen, Germany) with a built-in body coil. The phantoms were transported from the refrigerator to the MRI scanner within approximately 5 minutes, and scanning was initiated immediately. RF radiation from the transmission coil covered the area within an approximate 300 mm radius from the center of the static magnetic field (B_0). The scan table was positioned so that the center axis of the phantoms aligned with the center of the B_0 while scanning. For example, when scanning the head phantom, the scan table was adjusted so that the head phantom's center aligned with B_0. In our study, scanning was performed at 4 sites, where centers of B_0 were at one-third of the head, the center of the neck, one-third of the trunk, and two-thirds of the trunk (dotted lines in Fig. 3). The scan parameters we used are shown in Table 1 which were based on clinical parameters. These sequences are typically performed when conducting PMMRI in addition to postmortem CT at our institution, especially when performing whole-body MRI. The imaging was conducted in the order listed in Table 1, starting from the top. The controlled operating mode was used by setting the first-level controlled mode as the upper limit.

Measurement of whole-body average specific absorption rate (SAR)

Based on the information of DICOM (Digital Imaging and Communications in Medicine), the MRI system we used was capable of displaying "whole-body average SAR for 6 minutes" which was defined by the International Electrotechnical Commission (IEC) [14], and indicates how much energy is absorbed by the entire body during a 6-minute exposure period. With each MRI sequence we applied, whole-body average SAR was calculated by averaging the SAR for 6 minutes.

Table 1 Scan parameters of MRI used for head and trunk phantoms and their whole-body average SARs for 6 minutes

	Sequence	TR (ms)	TE (ms)	Thickness/ Gap (mm)	FOV (mm)	Time (min)	Whole-body average SAR for six minutes (W/Kg)
Head (axial)	T_2WI (TSE)	3200	88	6/1	220	1:47	0.23
	T_1WI (SE)	500	11	6/1	220	1:59	0.43
	PDWI (TSE)	2500	12	6/1	220	2:29	0.24
	T_2*WI (GE)	560	20	6/1	220	2:11	0.01
	Diffusion WI (EPI)	3300	106	6/1	220	1:04	0.05
	FLAIR (TSE)	9000	106	6/1	220	3:00	0.08
Neck (sagittal)	T_2WI (TSE)	3500	117	3/0.3	250	2:11	1.25
	T_1WI (TSE)	549	9.5	3/0.3	250	1:46	1.75
Heart (short axis)	Diffusion WI (EPI)	5000	117	4/0.4	220	3:47	0.51
	T_2WI (TSE)	5210	93	4/0.4	220	5:40	2.58
	T_2WI (3DTSE)	1200	100	1.2	200	6:09	0.20
Heart (4 chamber)	Diffusion WI (EPI)	5000	117	4/0.4	220	3:47	0.51
Thorax (coronal)	T_2WI (TSE)	3000	93	6/0.6	360	2:42	2.78
	T_1WI (GRE)	257	4.8	6/0.6	360	1:58	1.59
	STIR (TSE)	4970	65	6/0.6	360	2:29	3.86
Abdomen (coronal)	T_2WI (TSE)	3000	93	6/0.6	360	2:42	2.67
	T_1WI (GRE)	259	4.8	6/0.6	360	2:15	1.41
	STIR (TSE)	4970	65	6/0.6	360	2:29	4.00
						Total: 50:25	Average: 1.34

Abbreviations: 3D, 3-dimensional; EPI, echo planar imaging; FLAIR, fluid attenuated inversion recovery; FOV, field of view; GE, gradient echo; PD, proton density; SAR, specific absorption rate; SE, spin echo; STIR, short tau inversion recovery; TE, echo time; TR, repetition time; TSE, turbo spin echo; WI, weighted image

Statistical Analyses

On the graphs, temperatures (i.e. the dependent variable, y) at the 4 measured points on the phantoms were plotted at 5 minute-intervals during the 60-minute-scanning time and for 60 minutes after MRI (i.e. the independent variable, x). A linear regression of the relationship between temperature and time was calculated using the method of least squares [11]. The strength of the linear relationship between the two variables was quantified by calculating the correlation coefficient (r). SARs were shown as mean ± standard deviation. A repeated-measures analysis of variance (ANOVA) was performed to evaluate differences among the 4 measured points.

Statistical analysis was performed using Excel 2010 (Microsoft, Redmond, WA, USA) with the add-in software Statcel 2 (OMS publishing Inc, Tokorozawa, Saitama, Japan). A p-value of less than 0.05 was considered statistically significant. The correlation coefficient (r) was used to determine the strength of the correlation [15]: 0-0.19: very weak; 0.20-0.39: weak; 0.40-0.59: moderate; 0.60-0.79: strong; and 0.80-1.0: very strong.

Results

Setting the start time of MRI scan at 0 minutes, scanning of the head phantom (including the neck portion) finished at 26 minutes 22 seconds, the subsequent scanning of the trunk phantom started at 27 minutes 10 seconds, and finished at 61 minutes 34 seconds. The total MRI examination of 61 minutes 34 seconds contained the actual scanning time of 50 minutes 25 seconds, the time for positioning, and the time for tuning between each sequence (Table 1). Figs. 4-7 show temperature changes for 2 hours

measured every 5 minutes from immediately before MRI, during MRI, and for 60 minutes after MRI.

The temporal temperature changes during postmortem MRI scans were observed to evaluate the effects of RF energy exposure. The graph presented below illustrates the following points:

- "Start of head scan (0 min)": This marks the initiation of RF energy exposure during the head scan.
- "Start of trunk scan (27 min 10 sec)": This indicates the transition from head scanning to trunk scanning.
- "End of all scans (61 min 34 sec)": This marks the conclusion of RF energy exposure at the end of all scans.

The repeated-measures ANOVA revealed statistically significant differences among the anatomical regions ($p < 0.0001$). Post-hoc examination indicated that the head phantom significantly differed from three trunk phantoms, showing distinctly lower measurement values. No significant differences were observed among the three trunk phantoms.

In the head phantom, the relationship between temperature and time was expressed with the following equation (Fig. 4):

$$Temp = 0.032\ Time + 10.13\ (r = 0.998;\ P = 2.172 \times 10^{-29}) \quad \cdots\cdots\cdots (1)$$

, where *Temp* stands for temperature and r stands for the coefficient of determination (the same applies to the following formulas).

The temperature of the head phantom was 10.1℃ immediately before MRI, and 13.9℃ (the highest during the measurement) at 120 minutes after the start of MRI.

In the upper part of the trunk phantom, the relationship between temperature and time was expressed with the following equation (Fig. 5):

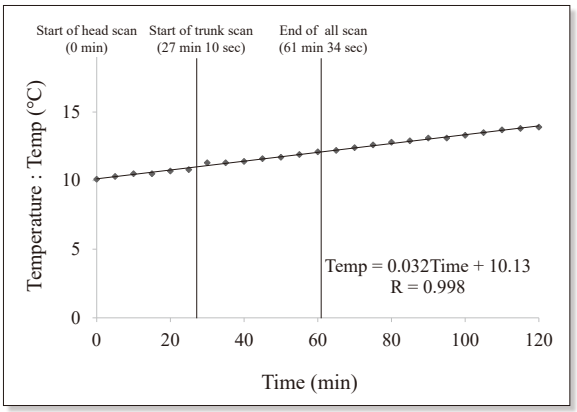

Fig. 4 Temperature of the head phantom measured at every 5 minutes
The solid line represents linear approximation.

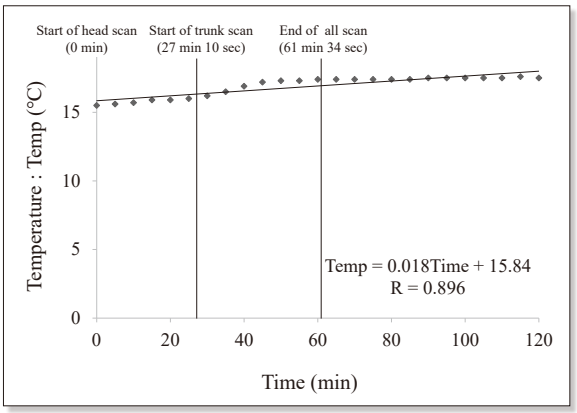

Fig. 5 Temperature of the upper trunk phantom measured at every 5 minutes
The solid line represents linear approximation.

$$Temp = 0.018\ Time + 15.84\ (r = 0.896;\ P = 1.447 \times 10^{-9}) \quad \cdots\cdots\cdots (2)$$

The temperature of the upper part of the trunk phantom was 15.5℃ immediately before MRI and 17.5℃ at 120 minutes after the start of MRI. The highest temperature during the 120-minute measurement was 17.6℃ at 115 minutes after the start of MRI. From 35 to 80 minutes after the start of MRI, the temperature of the upper trunk was higher than the approximated line created by the least squared method, with the maximum of 0.6℃ higher at 50 minutes.

In the middle part of the trunk phantom, the relationship between temperature and time

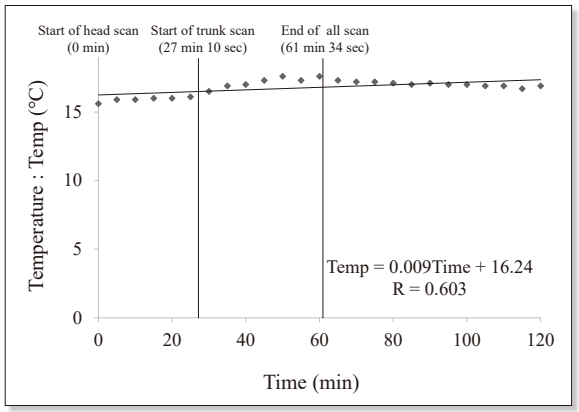

Fig. 6 Temperature of the middle trunk phantom measured at every 5 minutes
The solid line represents linear approximation.

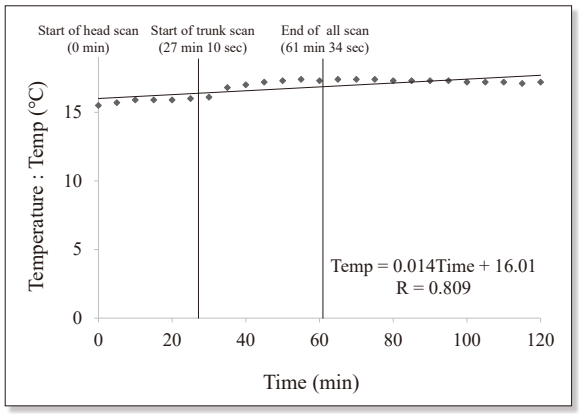

Fig. 7 Temperature of the lower trunk phantom measured at every 5 minutes
The solid line represents linear approximation.

was expressed with the following equation (Fig. 6):

$$Temp = 0.009\ Time + 16.24\ (r = 0.603;\ P = 1.411 \times 10^{-3}) \quad \cdots\cdots\cdots (3)$$

The temperature of the middle part of the trunk phantom was 15.6℃ immediately before MRI, and 16.9℃ at 120 minutes after the start of MRI. The highest temperature during the120-minute measurement was 17.6℃ at 50 and 60 minutes after the start of MRI. From 30 to 80 minutes after the start of MRI, the temperature of the middle part of the trunk phantom was higher than the approximated line created by the least squared method, with the maximum of 0.9℃ higher at 50 minutes.

In the lower part of the trunk phantom, the relationship between temperature and time was expressed with the following equation (Fig. 7):

$$Temp = 0.014\ Time + 16.01\ (r = 0.809;\ P = 1.701 \times 10^{-6}) \quad \cdots\cdots\cdots (4)$$

The temperature of the lower part of the trunk phantom was 15.5℃ immediately before MRI, and 17.2℃ at 120 minutes after the start of MRI. The highest temperature during the 120-minute measurement was 17.4℃ at 55, 65, 70, and 75 minutes after the start of MRI. From 35 to 85 minutes after the start of MRI, the temperature of the lower portion of the trunk was higher than the approximated line created by the least squared method, with the maximum of 0.6℃ higher at 55 minutes.

Whole body average SAR for 6 minutes ranged from 0.01 to 4.00 (1.34 ± 1.33) W/kg depending on the scanned part of the phantoms (Table 1).

Discussion

In our study, near surface temperatures in all measured points in the phantoms were almost proportional to the time throughout the measurement. However, the following 4 differences were noted between the results of the head phantom and the trunk phantom:

1) Immediately before MRI, the temperature of the head phantom (10.1℃) was lower than that of the trunk phantom's upper (15.5℃), middle (15.6℃), and lower (15.5℃) parts.
2) Inclination of the linear graph of the head phantom (0.032) was greater than that of the trunk phantom's upper (0.018), middle (0.009), and lower (0.014) parts.
3) The coefficient of determination (r) of the trunk phantom's upper (0.896), middle (0.603), and lower (0.809) parts was less than that of the head phantom (0.998).

4) The temperature of the trunk phantom was slightly higher than the line approximated by the least square method from 30 to 85 minutes after the start of MRI.

The phenomenon of the above-mentioned 1) and 2) can be explained by the surface-to-volume ratio (= the amount of surface area per unit volume). The larger the surface-to-volume ratio of an object, the more heat gain and loss occurs through the surface area. Generally, if the volume of an object is small, the surface-to-volume ratio increases; thus, it is easily affected by ambient temperature [16]. Since the volume of the head phantom was smaller than that of the trunk phantom, the head phantom was considered more susceptible to ambient temperature. Therefore, after keeping the phantoms in cold storage at 4℃ for 11 hours, the temperature of the head phantom before MRI was lower than that of the trunk phantom, and the subsequent temperature increase after having been moved out of the cold storage was considered greater. Similarly, Barton et al. measured surface temperature change of a corpse in the head, chest, and abdomen after taking the corpse out of refrigerated storage at 4℃, and reported that the head portion was more susceptible to ambient temperature change [17]. Additionally, in this study, the head phantom is surrounded by a 3 mm thick polypropylene wall, while the trunk phantom has a 12.5 mm thick acryl wall. This difference in thickness and material of the wall may have resulted in the head phantom having a higher thermal conductivity and experiencing more rapid temperature changes. Moreover, although the baseline temperature of both head and trunk phantoms did not exactly reach 4℃ despite the extended refrigeration period, the trunk phantom demonstrated nearly identical start temperatures and consistent temporal temperature changes across different measurement points. This indicates minimal inconsistencies in refrigeration conditions, suggesting that any potential non-uniformity in thermal equilibrium within the phantoms likely had negligible effects on the study outcomes.

The phenomenon of the above-mentioned 3) and 4) can be explained by SAR. In this study, the mean whole body average SAR of the phantoms was 1.34 W/kg and SAR of the head phantom was lower than the mean in each applied sequence. Furthermore, RF irradiation was considered not to have affected the head phantom during imaging of the trunk, because the distance from the measured point on the head phantom (① on Fig. 2) to the center of B_0 for the thorax and the heart site (Fig. 3) was 330 mm (150 + 180 mm), exceeding the RF radiation range (300 mm radius from the B_0 center). Consequently, the head phantom's temperature consistently increased at a stable rate due to ambient room temperature. In contrast, temperature increases observed in regions exposed to RF radiation were distinctly different during the respective imaging times. These differences in temperature behavior support the conclusion that observed temperature variations during imaging periods are primarily attributable to RF radiation exposure. Whereas, for the trunk phantom, 7 SARs of 10 imaging sequences were higher than the mean, and the examination time for the trunk phantom (33 minutes 58 seconds) was longer than for the head phantom (16 minutes 27 seconds). This difference can be attributed to the larger size of the trunk phantom, which affects the specific absorption rate (SAR). According to the equation $SAR = C\sigma r^2 Bo^2 \alpha^2 D$ (where C is a proportional constant, σ is the electrical conductivity, r is the effective radius, Bo is the magnetic field strength, α is the flip angle, and D is the duty cycle), SAR increases proportionally to the square of the radius (r^2) [18]. The larger size of the trunk phantom results in higher SAR values due to its greater interaction with the RF field. The temperature observed in the trunk phantom between the

"Start of trunk scan" and the "End of all scan" was slightly higher temperatures than the graph line approximated by the least squared method (Fig. 5-7), which was different from linearly increased head phantom's temperature (Fig. 4). This suggests that the trunk phantom's temperature increase was affected not only by the temperature of the room but also by SAR, or the RF energy emitted during the imaging process, as it showed a similar trend at all three measurement points in the trunk phantom. Sustained RF exposure was confirmed to cause significant and consistent temperature increases. In contrast, if the phantoms were kept at room temperature without RF exposure, no transient or pronounced temperature changes would be expected.

Our study has three limitations. First, we did not measure control data without RF irradiation. To accurately assess this effect, the phantom should be cooled again with its temperature measured in the MR room over the same time period, but without initiating an MRI scan. This experiment was not conducted due to the necessity of minimizing the time the equipment was occupied for clinical patient imaging, a limitation further exacerbated by institutional policies related to COVID-19. The original experiment was conducted in approximately 2020, during which the impact of COVID-19 precluded the possibility of performing control experiments. At present, relocation to a new facility has rendered the reproduction of the original experimental conditions impractical, further constraining our ability to conduct control experiments. Thus, we could not verify the extent of temperature increase due to the temperature of the room alone. Second, the phantom used in this study is homogeneous, which does not fully replicate the heterogeneous conditions of a human body. Therefore, the exact phenomena observed in this study may not be entirely reproducible in a real human body. Third, temperature measurements in this study were conducted at a depth of 1 cm to minimize evaporative cooling effects and ensure measurement stability. However, temperature changes at both surface and deeper tissue regions should also be evaluated to fully understand RF-induced heating effects. Additionally, the trunk phantom thickness used (180 mm) was thinner than typical human torso thicknesses (approximately 200–300 mm) due to structural constraints of the phantom container. Previous studies have reported postmortem changes in dielectric and conductivity properties, potentially increasing SAR by about 10% [19-21], which cannot be replicated in phantoms. Future studies should address these limitations by measuring temperatures at multiple depths, using phantoms more representative of actual human anatomy, and considering postmortem tissue property changes.

In conclusion, the RF energy-induced heating during PMMRI primarily affected superficial regions, consistent with known RF absorption patterns. The magnitude of temperature rise observed was modest. Consequently, the potential risk of surface tissue damage due to RF heating appears minimal. Nonetheless, considering the inherent differences between the phantom and actual postmortem conditions, these results should be interpreted with caution, and further in-vivo investigations may still be warranted to confirm the clinical safety implications of RF-induced temperature variations during PMMRI.

Conflict of interest

The authors declare no conflict of interest.

表の説明

Table 1　頭部および胴体ファントムに使用したMRIの撮像パラメーターおよび6分間の全身平均SAR

図の説明

Fig.1　頭部および胴体ファントムと4本の光ファイバー温度計
(a) MRIスキャナー内に配置した頭部および胴体ファントム．胴体ファントムには温度測定のために4本の光ファイバー温度計が挿入されている．(b, c) 本研究で使用した黒い頭部ファントムの拡大図．

Fig.2　ファントムの温度測定部
表面付近に設定した4つの温度測定部
① 頭部ファントム
② 胴体ファントムの上部
③ 胴体ファントムの中部
④ 胴体ファントムの下部

Fig.3　温度測定部と静磁場 (B_0) の中心位置 (4つの撮像部位)
各ファントムにおける静磁場の中心位置
頭部：首を除く頭部ファントムの上部3分の1
首：首の中央
胸部・心臓：胴体ファントムの上部3分の1
腹部：胴体ファントムの上部3分の2
(①②③④は温度測定部を示す)

Fig.4　5分ごとに測定した頭部ファントムの温度
実線は線形近似を示す．

Fig.5　5分ごとに測定した胴体ファントム上部の温度
実線は線形近似を示す．

Fig.6　5分ごとに測定した胴体ファントム中部の温度
実線は線形近似を示す．

Fig.7　5分ごとに測定した胴体ファントム下部の温度
実線は線形近似を示す．

References

1) Horsfall I., et al.: Forensic imaging: Developing applications of computed tomography and magnetic resonance imaging. Forensic Sci Med Pathol, 16(3), 477-489, 2020.
2) Jackowski C., et al.: Virtopsy: postmortem imaging of the human heart in situ using MSCT and MRI. Forensic Sci Int, 149(1), 11-23, 2005.
3) Okuda T., et al.: A case of fatal cervical discoligamentous hyperextension injury without fracture: Correlation of postmortem imaging and autopsy findings. Forensic Sci. Int, 225(1-3), 71-74, 2013.
4) Thayyil S., et al.: Post-mortem MRI versus conventional autopsy in fetuses and children: a prospective validation study. The Lancet, 382(9888), 223-233, 2013.
5) Brix G., et al.: Sampling and evaluation of specific absorption rates during patient examinations performed on 1.5-Tesla MR systems. Magnetic resonance imaging, 19, 6, 769-79, 2001.
6) Shellock, F.G., et al.: Thermal effects of high-field (1.5 tesla) magnetic resonance imaging of the spine. Clinical experience above a specific absorption rate of 0.4 W/kg. Acta radiologica Supplementum, 369, 514-6, 1986.
7) Shellock, F.G.: Radiofrequency energy-induced heating during MR procedures: a review. J Magn Reson Imaging, 12(1), 30-6, 2000.
8) Shellock, F.G., et al.: Temperature, heart rate, and blood pressure changes associated with clinical MR imaging at 1.5 T. Radiology, 163, 259-262, 1987.
9) Tang, M., et al.: Progress in understanding radiofrequency heating and burn injuries for safer MR imaging. Magn Reson Med Sci, 22, 7-25, 2023.
10) Shellock, F.G., et al.: Temperature changes caused by MRI of the brain with a head coil. AJNR, 9, 287-291, 1988.
11) Kobayashi, T., et al.: Skin temperature increase after whole body postmortem magnetic resonance imaging. Forensic Imaging, 200405, 2020.
12) ASTM F2182-09: Standard test method for measurement of radio frequency induced heating on or near passive implants during magnetic resonance imaging. West Conshohocken, PA: ASTM International, 2009.
13) Zhang, J., et al.: Effects of tissue preservation temperature on high strain-rate material properties of brain. J Biomech, 44(3), 391-396, 2011.
14) International Electrotechnical Commission (IEC): Medical electrical equipment, part 2: particular requirements for the basic safety and essential performance of magnetic resonance equipment for medical diagnosis. IEC, 60601-2-33, 2010.
15) Sedgwick, P.: Pearson's correlation coefficient. British Medical Journal, 345, 41-56, 2012.
16) Planinsic, G., et al.: The surface-to-volume ratio in thermal physics: from cheese cube physics to animal metabolism. Eur J Phys, 29, 369-384, 2008.
17) Barton, P.S., et al.: Temperature dynamics in different body regions of decomposing vertebrate remains. Forensic Sci Int, 110900, 2021.
18) Röschmann, P.: Radiofrequency Penetration and Absorption in the Human Body: Limitations to High-Field Whole-Body Nuclear Magnetic Resonance Imaging. Medical Physics, 14(6), 922-931, 1987.
19) WANG, Lei., et al.: Dielectric properties of human active liver, kidney and spleen compared to those of respective inactive tissues, porcine tissues and the data provided by a database in the frequency range of 10 Hz to 100 MHz. IEEE trans biomed eng, 68(10), 3098-3109, 2021.
20) CANTÜRK, İsmail., et al.: An experimental evaluation of electrical skin conductivity changes in postmortem interval and its assessment for time of death estimation. Comput Biol Med, 69, 92-96, 2016.
21) Schmid, G., et al.: Dielectric properties of human brain tissue measured less than 10 h postmortem at frequencies from 800 to 2450 MHz. Bioelectromagnetics, 24(6), 423-30, 2003.